

# RSC Advances



This is an *Accepted Manuscript*, which has been through the Royal Society of Chemistry peer review process and has been accepted for publication.

*Accepted Manuscripts* are published online shortly after acceptance, before technical editing, formatting and proof reading. Using this free service, authors can make their results available to the community, in citable form, before we publish the edited article. This *Accepted Manuscript* will be replaced by the edited, formatted and paginated article as soon as this is available.

You can find more information about *Accepted Manuscripts* in the [Information for Authors](#).

Please note that technical editing may introduce minor changes to the text and/or graphics, which may alter content. The journal's standard [Terms & Conditions](#) and the [Ethical guidelines](#) still apply. In no event shall the Royal Society of Chemistry be held responsible for any errors or omissions in this *Accepted Manuscript* or any consequences arising from the use of any information it contains.



## Effects of metal promotion on CuMgFe catalysts derived from layered double hydroxides for higher alcohols synthesis via syngas

Xinyou Han,<sup>a,b</sup> Kegong Fang<sup>\*a</sup> and Yuhan Sun<sup>\*a,c</sup>

Received 00th January 20xx,  
Accepted 00th January 20xx

DOI: 10.1039/x0xx00000x

www.rsc.org/

Cu-Mg-Fe-M-O (M=Mn, Zr, Ce) catalysts derived from layered double hydroxides (LDHs) precursors were prepared using co-precipitation method and tested for higher alcohol synthesis (HAS) via carbon monoxide hydrogenation. The catalysts were subsequently characterized by N<sub>2</sub>-physisorption, X-ray diffraction (XRD), transmission electron microscopy (TEM), X-ray photoelectron spectroscopy (XPS) and H<sub>2</sub> temperature-programmed reduction (H<sub>2</sub>-TPR). The results show that Mn, Zr and Ce promoters mainly contribute to the formation of octahedrally coordinated copper species which favor for the enhancement of the total alcohol selectivity. The addition of Mn facilitates the interaction between Cu and Fe which causes the total alcohol selectivity and C<sub>2+</sub> alcohol content in the total alcohols to increase from 9.82% and 68.85% to 15.16% and 73.14% respectively. However, the addition of Zr and Ce weakens the Cu-Fe interaction but increases the possibility of contact between Cu and Fe. As a consequence, the total alcohol selectivity is enhanced while C<sub>2+</sub> alcohol content in the total alcohols is reduced upon Zr and Ce addition. Based on the characterizations and catalytic results of the catalysts, a triple-active-site model is proposed to explain the different promoting effects of the three additives.

### 1. Introduction

Under the limited crude oil reserves and severe polluting circumstance recent years, effective catalytic transformation of alternative and renewable carbon sources to clean energy carriers and chemical feedstocks become both urgent and promising issues<sup>1</sup>. The higher alcohols synthesis (HAS) from coal or natural gas via syngas became an attracting subject for both industrial application and fundamental research due to its potential application as fuels, octane booster, or valuable chemical intermediates<sup>2</sup>. Till now, various catalyst systems have been developed to synthesize higher alcohols from syngas, including (I) the modified methanol catalysts<sup>3-5</sup>, (II) the modified Fisher-Tropsch (F-T) catalysts (Cu-Fe, Cu-Co based catalysts), (III) the Mo-based catalysts<sup>10, 11</sup> and (IV) the supported noble metal catalysts<sup>12, 13</sup>. Among these catalyst systems available for HAS from syngas, Cu-Fe based catalyst is considered as a promising system due to its higher C<sub>2+</sub> alcohol content in the total alcohols than modified methanol catalyst, less harsh reactive conditions than Mo-based catalyst, and much lower cost than the supported noble metal catalyst. According to the earlier studies<sup>7, 14, 15</sup>, Fe could induce the

dissociative adsorption of CO and hydrogenation as the carbon chain growth site, while Cu performs as CO insertion site through facilitating the dissociative chemisorption of H<sub>2</sub> and the associative adsorption of CO. As the production of mixed alcohols requires cooperation of chain-growth and CO insertion active sites<sup>7, 14</sup>, the synergistic effect between Cu and Fe is vitally important in the HAS reactions. Recent research<sup>16-18</sup> demonstrate that there are still many problems exist for the Cu-Fe based catalysts, such as copper sintering at high temperature and high selectivity to relatively cheaper hydrocarbons, which result in deactivation of catalysts and undermining the economic efficiency of carbon monoxide conversion, respectively. In order to improve the performances of the Cu-Fe based catalytic system, many promoters<sup>5, 14, 19-22</sup> such as Zn, Mn, Zr, Ce have been introduced into the catalysts system. It is found that the catalysts with higher Cu dispersion, stronger Cu-Fe synergistic effect could achieve better catalytic performance for HAS. However, some of the intrinsic issues like the effect of copper reduction temperature on the catalytic performances among different promoters and the mechanisms of how the additives promote the HAS process as well as the synergistic effect between Cu and Fe are still confusing. Therefore, more detailed research over the model catalysts is needed to explain the promoting effect and the synergistic role of the many different efficient additives in the HAS from syngas.

Recently, much attention has been paid to the layered double hydroxides (LDHs) materials as heterogeneous catalysts or supports due to their versatility in chemical composition and structural architecture. In the layered structure of the LDHs, metal ions mixed with each other homogeneously, creating a

<sup>a</sup> State Key Laboratory of Coal Conversion, Institute of Coal Chemistry, Chinese Academy of Sciences, Taiyuan 030001, Shanxi, China

<sup>b</sup> University of the Chinese Academy of Sciences, Beijing 100039, China

<sup>c</sup> Shanghai Advanced Research Institute, Chinese Academy of Sciences, Shanghai 201203, China

\*Corresponding author:

Kegong Fang E-mail addresses: kgfang@sxicc.ac.cn Yuhan Sun E-mail addresses:

sunyh@sari.ac.cn Tel: +86-(0)351 4064505 Fax: +86-(0)351 4041153

Electronic Supplementary Information (ESI) available: See

DOI: 10.1039/x0xx00000x

homogeneous system. Early research<sup>23, 24</sup> have demonstrated that the Cu ions could be highly dispersed in LDHs structure. Besides, under calcination or reducing conditions, the topotactic transformation of LDHs materials to metal-metal oxides could be of great significance for Cu-Fe based catalysts with different metal promoters.

Herein, a series of model catalysts derived from the LDHs with Mn, Zr, and Ce as additives are synthesized in this work. The relationship between the physical-chemical properties and the catalytic performance for HAS of as-prepared catalysts are discussed. Furthermore, the mechanism of how the additives affect the synergistic effect between Cu and Fe are studied based on a triple-active-site model in order to explain the promoting effect of the additives on the catalytic behavior of catalysts in HAS process.

## 2. Experimental

### 2.1 Catalyst preparation

The Cu-Mg-Fe-M-O (M=Mn, Zr, Ce) catalysts derived from LDHs were prepared by precipitation-hydrothermal method. The calculated amount of  $\text{Cu}(\text{NO}_3)_2 \cdot 3\text{H}_2\text{O}$ ,  $\text{Fe}(\text{NO}_3)_3 \cdot 9\text{H}_2\text{O}$ ,  $\text{Mg}(\text{NO}_3)_2 \cdot 6\text{H}_2\text{O}$  and  $\text{M}(\text{NO}_3)_x \cdot n\text{H}_2\text{O}$  (M=Mn, Zr, Ce) were dissolved together in 400 mL deionized water ( $[\text{Cu}^{2+}] + [\text{Mg}^{2+}] + [\text{Fe}^{3+}] + [\text{M}^{n+}] = 0.3 \text{ M}$ ), which was referred as solution A. Solution B was KOH solution with concentration of 0.8M. Solutions A and B were simultaneously added into a glass reactor under vigorous stirring at room temperature and a pH value of about 10.

The result suspension was transferred into a stainless autoclave (1000 mL) equipped with a Teflon inner layer, put into an oil bath, and aged at 100°C for 12h under stirring, filtered off, and washed thoroughly with distilled water. The precipitate was then dried at 80°C overnight. The resulting powder was calcined under air at 673 K for 3 h to get the  $\text{CuMg}_2\text{Fe}_{0.8}\text{M}_{0.2}\text{O}_x$  (M=Mn, Zr, and Ce) catalysts with the subscripts as the nominal composition. For simplification, the obtained catalysts were denoted as CMF, CMF-Mn, CMF-Zr, and CMF-Ce, respectively.

Typically, a mixture of copper, iron and magnesium nitrate with the same composition of CMF catalyst was precipitated with an aqueous solution of  $\text{K}_2\text{CO}_3$  at room temperature and a constant pH of 7-8 in a well-stirred thermo-stated container. After aging at 100°C for 12h, the precipitate was washed thoroughly with distilled water, and dried at 80°C overnight. The calcination process followed the same procedure described above (denoted as CMF-NL).

### 2.2 Characterizations

The specific surface area and pore volume of samples were detected using  $\text{N}_2$  adsorption-desorption isotherms (Micromeritics ASAP-2000). The bulk structures of the samples before and after calcination were measured by XRD (Rigaku D/max-RA, Cu  $\text{K}\alpha$  radiation,  $\lambda = 1.542 \text{ \AA}$ ). X-ray photoelectron spectra (XPS) were recorded on a Thermo VGESCALAB250 X-ray photoelectron spectrometer at a pressure of  $2 \times 10^{-9} \text{ Pa}$  using Al  $\text{K}\alpha$  X-ray as the excitation source.  $\text{H}_2$  temperature-

programmed reduction ( $\text{H}_2$ -TPR) was carried out in a quartz reactor at atmospheric pressure. Sample (0.03 g) was loaded in the middle of the reactor tube which was purged with  $\text{N}_2$  at 473 K for 1 h. Then a reductive gas (5%  $\text{H}_2/\text{Ar}$ ) was introduced at a flow rate of  $30 \text{ mL min}^{-1}$ . The temperature of the reactor was augmented linearly from 373 to 1173 K with a ramp of  $10 \text{ K min}^{-1}$  using a temperature-programmed controller.

### 2.3 Catalytic evaluation

Samples (1.0 mL, 40-60 mesh) equivalently diluted with quartz granules were evaluated in a pressured fixed-bed reactor at 513 K, 4.0 MPa,  $5000 \text{ h}^{-1}$  with a  $\text{H}_2/\text{CO}$  ratio of 2:1. Prior to the reaction, the catalysts were reduced in situ in a flow of syngas ( $\text{H}_2/\text{CO}$  ratio of 2:1,  $40 \text{ mL min}^{-1}$ ) under atmospheric pressure at 523 K for 8h. The effluents gases were analyzed using Carbosieve-packed column with TCD and  $\text{Al}_2\text{O}_3$  column with flame ionization detector (FID). Propake-Q column with TCD and FID were applied to the analysis of water, methanol and other alcohol products in liquids.

## 3. Results and discussion

### 3.1 $\text{N}_2$ -adsorption

Fig. 1(a) presents the nitrogen adsorption-desorption isotherms of CMF, CMF-Mn, CMF-Zr, and CMF-Ce catalysts. All the four samples exhibit a typical IV isotherms according to the IUPAC classification with an  $\text{H}_2$ -type hysteresis loop, indicating the presence of mesopores like "ink bottles" which might be formed by the accumulation of uniform particles. The BET surface area, pore diameter and pore volume of these samples (calculated from adsorption isotherms) are

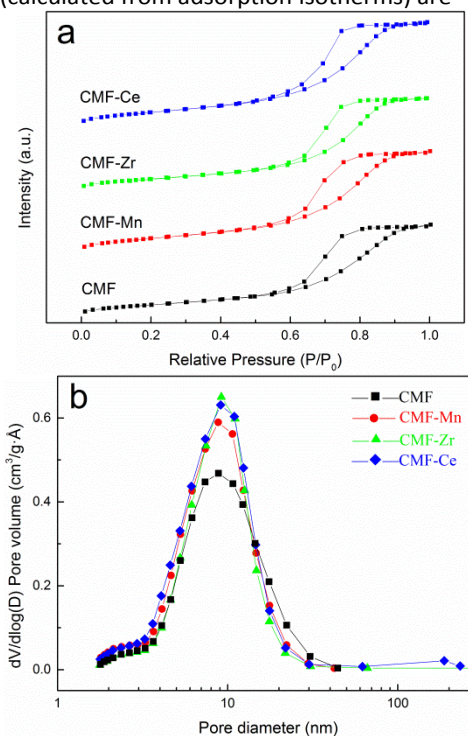


Fig. 1 (a) The  $\text{N}_2$  physisorption isotherms and (b) the pore size distribution patterns of the CMF catalysts with different additives

**Table 1**

Textural parameters of the samples

Catalyst	$S_{\text{BET}}$ ( $\text{m}^2/\text{g}$ )	$D_p$ (nm)	$V_p$ ( $\text{cm}^3/\text{g}$ )
CMF	114.5	7.96	0.27
CMF-Mn	140.5	7.31	0.30
CMF-Zr	122.2	7.71	0.28
CMF-Ce	145.8	7.44	0.31

$S_{\text{BET}}$ : BET surface area;  $D_p$ : pore diameter;  $V_p$ : pore volume

summarized in Table 1. It can be seen that the addition of Mn, Zr, and Ce all contribute to the increase of the BET surface area and the pore volumes of catalysts while the average pore diameter decreases. This result is further confirmed by the corresponding pore size distribution (Fig. 1 b) in which the increase of pore volumes is very clear. As the existence of unconsolidated pores formed by the accumulation of uniform particles discussed above, the increase of pore volumes and decrease of pore diameters (Table 1) can be attributed to the decrease of crystal size of catalysts particles because of the addition of promoters, which will be discussed in 3.3 section.

### 3.2 X-ray diffraction

XRD patterns of the as-prepared CMF-M catalysts before and after calcination are shown in Fig. 2. Before calcination the catalysts are all have a characteristic (003) reflection peak of LDHs at  $2\theta$  of  $11.3^\circ$ . It is noticed that the addition of Ce result in the decrease of crystallinity of LDHs evidently and this may attribute to the ionic radii of  $\text{Ce}^{3+}$  (0.102 nm) is much bigger than that of  $\text{Mg}^{2+}$  (0.072nm) or  $\text{Fe}^{3+}$  (0.055nm) ions. As for the addition of  $\text{Mn}^{2+}$  (0.067nm) and  $\text{Zr}^{4+}$  (0.072nm), the intensity of (003) peak changes less compared to that of CMF catalyst. It

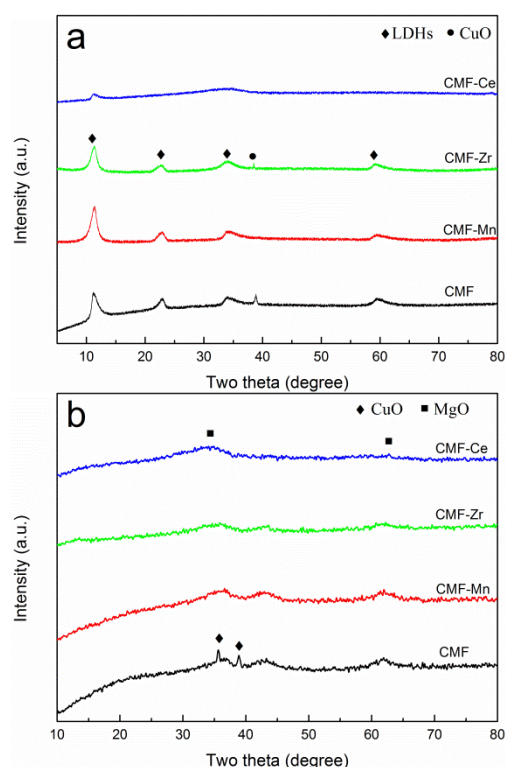


Fig. 2 XRD patterns of the as-synthesized catalysts (a) before and (b) after calcination

also can be seen that none of these catalysts are ever found any diffraction peaks of separated Mn, Zr, or Ce species except the reflection peaks of LDHs and CuO, indicating that  $\text{Mg}^{2+}$  or  $\text{Fe}^{3+}$  ions in brucite-like layers of LDHs are replaced by the doped metal ions<sup>23</sup>.

After calcination, only the CMF catalyst shows the characteristic CuO reflection peaks. None of the other three samples shows any peaks of CuO or other species, which are basically amorphous phases, indicating that the metal ions are all homogeneously dispersed. Agreed with the  $\text{N}_2$  physisorption results, the XRD spectra indicates that the three kinds of additives (Mn, Zr, and Ce) all could contribute to the formation of smaller catalysts particles, moreover inhibit the sintering of copper species in the hydrothermal and calcination process.

### 3.3 TEM

Fig. 3 shows TEM images of the CMF-M catalysts. Agreed with the  $\text{N}_2$ -adsorption result, all of the catalysts exhibit mesoporous structure which are formed by the accumulation of uniform particles. Moreover, from the particle size distribution of the four catalysts showed in the images, it is observed that after adding additives, the average particle size of the catalysts decreased from 6.1nm(CMF) to 4.2nm(CMF-Mn), 4.5nm(CMF-Zr), and 4.6nm(CMF-Ce) respectively.

### 3.4 XPS

To investigate the surface chemistry of the catalysts and understand the synergistic effect between Cu and Fe, XPS of Cu 2p and Fe 2p were performed and the result spectra with fitting curves are illustrated in Fig. 4. The quantitative analysis of the Cu 2p and Fe 2p signals for the CMF-M (M=Mn, Zr, Ce) catalysts are shown in Table 2 and 3.

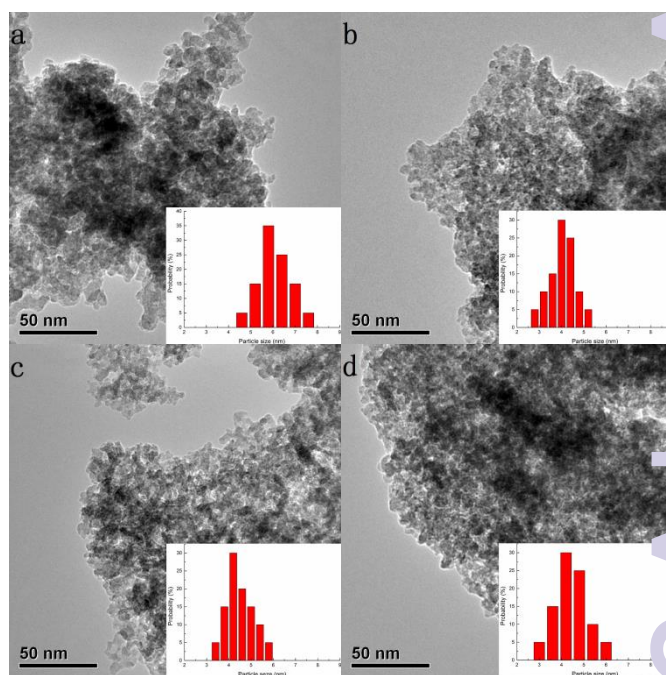


Fig. 3 TEM images of the CMF-M catalysts with different additives (a, CMF; b, CMF-Mn; c, CMF-Zr; d, CMF-Ce)

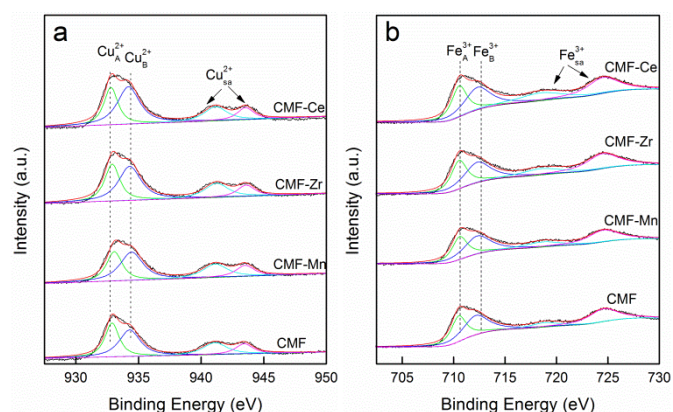


Fig. 4 XPS spectra of the (a) Cu 2p and (b) Fe 2p regions in the CMF-M (M=Mn, Zr, Ce) catalysts

According to early reports by Li and Lenglet<sup>25, 26</sup>, it is possible to distinguish between tetrahedrally ( $\text{Cu}_A^{2+}$ , CuO species) and octahedrally ( $\text{Cu}_B^{2+}$ ) coordinated  $\text{Cu}^{2+}$  cations. In this study, from the results of quantitative analysis of the Cu 2p in Table 2, it can be seen that after introduction of metal ions into the Cu-Mg-Fe catalytic system, the surface composition of the catalysts experienced clear change compared to CMF catalyst. The content of octahedrally coordinated  $\text{Cu}^{2+}$  cations in the three catalysts (CMF-Mn, CMF-Zr, and CMF-Ce) all increase because of the addition of promoters, indicating that the addition of three metals all could inhibit the CuO sintering. In other words, the three additives contribute to the highly dispersion of Cu through facilitating interaction between Cu and the other active components in the octahedral void. Moreover, the three additives also result in the change of chemical environments of  $\text{Cu}^{2+}$ . As is shown, the binding energies of  $\text{Cu}_A^{2+}$  and  $\text{Cu}_B^{2+}$  in CMF-Mn catalyst are all increase compared to CMF catalyst which could be attributed to the strong interaction between Cu and the introduced Mn species. However, phenomenon is different for CMF-Zr and CMF-Ce catalysts in which the binding energies of  $\text{Cu}_A^{2+}$  and  $\text{Cu}_B^{2+}$  decrease compared to that of CMF catalyst, which reveals the weak interaction between Cu and Fe.

**Table 2**

XPS characteristics of Cu 2P region for the CMF-M

Catalyst	Binding energy(eV)		Peak intensity (%)	
	$\text{Cu}_A^{2+}$	$\text{Cu}_B^{2+}$	$I(\text{Cu}_A^{2+})$	$I(\text{Cu}_B^{2+})$
CMF	932.89	934.31	46.26	53.74
CMF-Mn	933.08	934.46	42.64	57.36
CMF-Zr	932.86	934.26	42.08	57.92
CMF-Ce	932.81	934.21	38.87	61.13

**Table 3**

XPS characteristics of Fe 2P region for the CMF-M

Catalyst	Binding energy(eV)		Peak intensity (%)	
	$\text{Fe}_A^{3+}$	$\text{Fe}_B^{3+}$	$I(\text{Fe}_A^{3+})$	$I(\text{Fe}_B^{3+})$
CMF	710.57	712.22	44.69	55.31
CMF-Mn	710.55	712.27	43.21	56.79
CMF-Zr	710.61	712.39	46.01	53.99
CMF-Ce	710.50	712.29	45.34	54.66

As for the Fe2p results which also suggests the coexistence of two kinds of  $\text{Fe}^{3+}$  ( $\text{Fe}_A^{3+}$  and  $\text{Fe}_B^{3+}$ ), the binding energies of  $\text{Fe}_B^{3+}$  all increase with the addition of promoters, indicating stronger interaction between iron and the other metals. However, the content of  $\text{Fe}_B^{3+}$  in CMF-Zr and CMF-Ce decrease compared to that of CMF which means that the addition of Zr and Ce decrease the dispersion of Fe content (Here  $\text{Fe}_B^{3+}$  should not refer to the Fe species contact with Cu because of the possible existence of  $\text{MgFe}_2\text{O}_4$ <sup>27</sup>). The addition of Zr and Ce result in the increase of  $\text{Fe}_A^{3+}$  ( $\text{Fe}_2\text{O}_3$ ) species. This may be due to that part of  $\text{Fe}^{3+}$  ions in catalysts are replaced by the Zr and Ce ions.

### 3.5 Reductive behavior

In order to take a further insight into the functions of the different additives and their effects on the catalysts,  $\text{H}_2$ -TPR of the four catalysts is performed. As is shown in Fig 5, two reduction processes are observed at low and high temperature range<sup>17, 22, 28</sup>. The strong reduction peak in the low temperature range (473K-673K) is mainly ascribed to the reduction of  $\text{CuFe}_2\text{O}_4$  to metallic Cu and  $\text{Fe}_3\text{O}_4$  while the peak in the high temperature range (>700K) could be assigned to the continuous reduction of Fe oxides to metallic Fe via FeO. To get more insight into the TPR results, the profiles from 473 to 673K which is mainly the reduction peaks of copper species are deconvoluted into several Gaussian peaks. The peak positions and their contributions derived from deconvolution are summarized in Table 4.

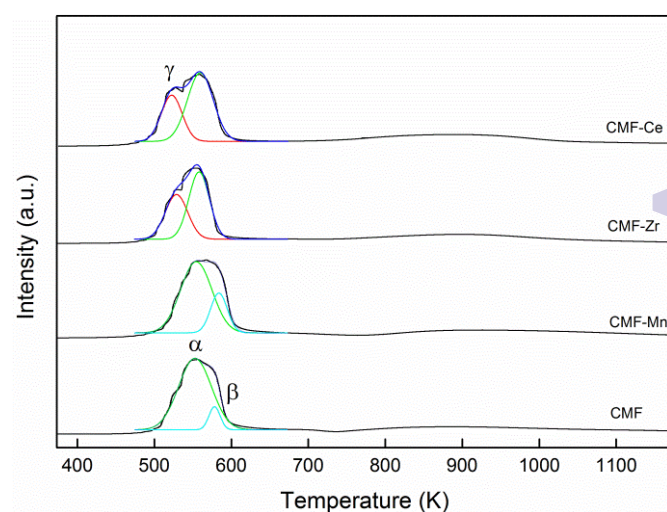


Fig. 5  $\text{H}_2$ -TPR profile of the CMF-M catalysts with different additives

**Table 4**

Center of reduction peaks and their contributions to the TPR pattern

Catalyst	TPR peak position [temperature (K)] and concentration (%) <sup>a</sup>		
	Peak $\alpha$	Peak $\beta$	Peak $\gamma$
CMF	552.6(90.00)	577.9(10.00)	—
CMF-Mn	554.0(77.04)	583.4(22.96)	—
CMF-Zr	557.9(57.98)	—	528.6(42.02)
CMF-Ce	558.4(64.93)	—	521.2(35.07)

<sup>a</sup> Values in parentheses are the contributions (%) of each species.

The peaks  $\alpha$  and  $\beta$  should be ascribed to the two reduction stages<sup>8</sup> of  $\text{CuFe}_2\text{O}_4$ : the low-temperature peak (peak  $\alpha$ ) is due to the reduction of Cu species in  $\text{CuFe}_2\text{O}_4$  to metallic Cu, it is noticed that the area of peak  $\beta$  in CMF-Mn catalyst is larger than peak  $\beta$  in CMF catalyst, which should be ascribed to the formation of  $\text{CuMn}_2\text{O}_4$  and the strong interaction between Cu and Mn. The strong interaction of Cu-Mn is also observed in the XPS result, moreover, agreed with the XPS result in which showed the strong interaction of Fe-Zr and Fe-Ce, peak  $\beta$  can hardly be observed in CMF-Zr and CMF-Ce catalysts. There also exists another peak at lower temperature (peak  $\gamma$ ) on the CMF-Zr and CMF-Ce catalysts, which can be assigned to the reduction of highly dispersed CuO. This highly dispersed CuO may be formed due to the strong interaction of Fe-Ce and Fe-Zr which result in the weak interaction between Cu and Fe. Hence, it can be concluded that the addition of Mn contributes to the stronger interaction between Cu and the other metal ions and result in the stronger synergistic effect. As for the addition of Zr and Ce, they mainly favor for the contact between copper and iron by facilitating the formation of highly dispersed copper species while the interaction of Cu-Fe becomes weaker because of the strong interaction between the additives (Zr, Ce) and Fe.

### 3.6 HAS performances of catalysts

The catalytic performances of the CMF-M (M=Mn, Zr, Ce) catalysts towards CO hydrogenation were examined under the following reaction conditions: 4.0 MPa, 513K, GHSV of  $5000 \text{ h}^{-1}$ ,  $n(\text{H}_2)/n(\text{CO}) = 2.0$ , in comparison with the CMF-NL catalyst. The CO conversion, selectivity towards total alcohols, hydrocarbons,  $\text{CO}_2$ , and the alcohols distribution are presented in Table 5.

It is clear that CMF-NL catalyst exhibits a low activity (CO conversion: 21.48%) and total alcohol selectivity (7.10%). In contrast, the CMF catalyst exhibit enhanced catalytic behaviour: the total alcohol selectivity increases gradually from 7.10% (CMF-NL) to 9.82% (CMF). Furthermore, the lower C2+ alcohol content in the total alcohols is observed over CMF-NL (57.58%) catalyst than CMF catalyst (68.85%), indicating enhanced Cu-Fe synergistic effect and Cu-Fe interaction in LDHs structure than amorphous phase. It can be seen that CMF-Mn, CMF-Zr, and CMF-Ce catalysts all show higher total alcohols selectivity compared to CMF catalyst. CMF-Ce catalyst shows the highest total alcohol selectivity with large amount of methanol formation while CMF-Mn catalyst exhibits the highest C2+ alcohol content in the total alcohols. This is agreed

with the early reports<sup>14, 20, 29-31</sup> in which show the increase of C2+ alcohol content in the total alcohols by introducing Mn promoter into the catalytic system. From the  $\text{CO}_2$  selectivity, it can be found that CMF-Mn shows the highest  $\text{CO}_2$  selectivity, indicating the enhancement of WGS effect or alcohol reforming reaction. However, the  $\text{CO}_2$  selectivity for CMF-Zr and CMF-Ce catalysts are much lower than that for CMF catalyst, this may be attributed to their strong interaction with Fe which could suppress the WGS reaction over the catalyst. As a whole, the catalytic results indicate that the three additives exhibit different promoting effect for the HAS reaction.

The different behaviours of the additives are also observed in the surface chemical phenomenon of the catalysts. Fig. 6 shows the relationship between the catalytic performances and the binding energies of the Cu ions. Interesting result is found that the CMF, CMF-Zr, and CMF-Ce catalysts could form a good linear relationship except for CMF-Mn. With the decrease of binding energies of  $\text{Cu}_B^{2+}$  because of the addition of Zr and Ce promoter, the total alcohol selectivity and methanol formation increases. However, the result is different for Mn promoter which causes the increase of binding energies of  $\text{Cu}_B^{2+}$  and the increase of alcohol selectivity. This also suggests that Mn plays a different role compared to Zr and Ce promoters in the HAS process.

Besides the different behaviors of affecting the physical-chemical properties of the catalysts, there are still some similarities of the three additives. Fig. 7 shows the relationship between alcohols selectivity and octahedrally coordinated copper contents. Good linear relationship between alcohols selectivity and octahedrally coordinated copper contents for the promoted catalysts is observed, meaning that more octahedrally coordinated copper species is favorable for the alcohol synthesis. The linear relationship also indicates that octahedrally coordinated copper species maybe the precursor of main active site for CO insertion in HAS process. Octahedrally coordinated copper species represents the existence of highly dispersed copper species which are of great significance for the formation of active sites for alcohol synthesis includes methanol and C2+ alcohols.

As for the different alcohols selectivity and product distribution after adding additives, the model showed in Fig. 8 may explain the promoting effect through the transition from the traditional dual-active-site to a triple-active-site of the catalyst system. In the picture the red arrow refers to the

**Table 5**

Catalytic performances of the catalysts

Cat	CO conversion (%)	STY <sub>ROH</sub> (g/ml/h)	Selectivity (wt. %)			Alcohol distribution (wt. %)	
			ROH	CHn	CO <sub>2</sub>	C1	C2+
CMF-NL	21.48	0.03	7.10	58.42	34.48	42.42	57.58
CMF	23.80	0.04	9.82	53.66	36.52	31.15	68.85
CMF-Mn	26.91	0.05	15.15	45.02	39.83	26.86	73.14
CMF-Zr	25.23	0.04	16.10	58.91	24.99	38.45	61.55
CMF-Ce	26.24	0.07	22.74	62.36	14.90	49.16	50.84

Reaction condition:  $\text{H}_2/\text{CO}=2$ , GHSV= $5000 \text{ h}^{-1}$ , T=513K, P=4.0MPa

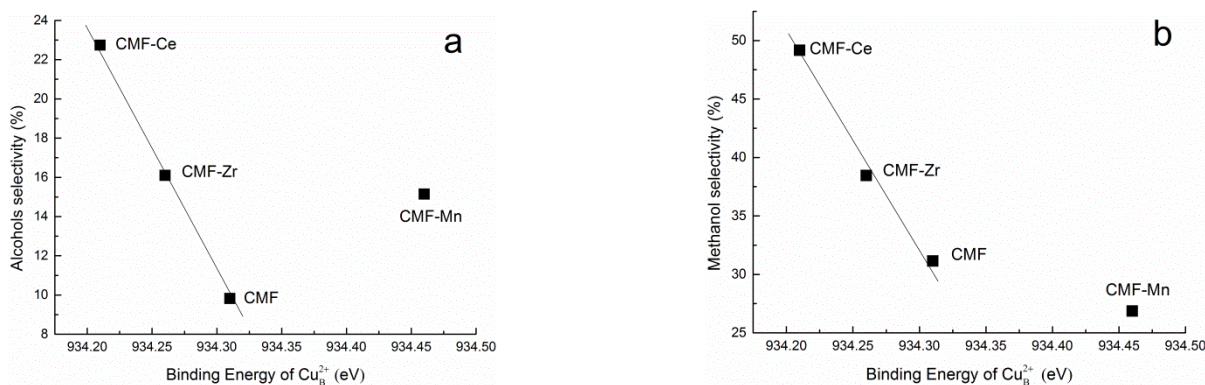


Fig. 6 Relationship between (a) alcohol selectivity and binding energy of  $\text{Cu}_B^{2+}$ , (b) Relationship between methanol selectivity and binding energy of  $\text{Cu}_B^{2+}$

strong interaction and the yellow arrow refers to the weaker interaction. For CMF-Mn catalyst, the strong interaction of Cu-Fe and Cu-Mn exist at the same time which would result in the increase of binding energies of  $\text{Cu}_B^{2+}$ . This strong interaction could also be seen in the TPR result which shows the increase of copper species reduced at higher temperature. The CMF-Mn catalyst shows the highest C2+ alcohol content in the total alcohols of the catalysts which also imply that Mn ions promote the increase of chain-growth sites of the catalyst.

For CMF-Zr and CMF-Ce catalysts, the Zr and Ce additives have a much stronger interaction with Fe than that with Cu which could be proved by the increase of binding energies of  $\text{Fe}_B^{3+}$  compared to CMF catalyst. This strong interaction results in the decrease of interaction between Cu and Fe, which is shown in the binding energies of  $\text{Cu}_B^{2+}$ . The strong interaction may be attributed to the formation of solid solution according to early report<sup>21, 22, 32-34</sup> in which also showed the strong interaction of Fe-Zr and Fe-Ce. However, the addition of Zr and Ce also contribute to the highly dispersion of Cu (see TPR

result in Fig. 5) and the formation of  $\text{Cu}_B^{2+}$  species is favorable for higher alcohol synthesis. Besides the structural effect, other reports<sup>5, 35</sup> also show the similar performances of Zr and Ce in the reduced catalysts:  $\text{Cu} + \text{M}^{n+} \rightarrow \text{Cu}^+ + \text{M}^{(n-1)+}$  ( $\text{M} = \text{Zr}^{4+}$  and  $\text{Ce}^{4+}$ ). The so formed  $\text{Cu}^+$  species could stabilize the nearby oxygenate intermediates and further contribute to the formation of the higher alcohols over CMF-Zr and CMF-Ce catalysts as well as the low  $\text{CO}_2$  selectivity compared to those over CMF catalyst.

In conclusion, the addition of Mn contributes to the formation of more strong synergistic effect between Cu and Fe while Zr and Ce behave on the contrary. In other words the addition of Mn mainly increases the chain-growth sites while the addition of Zr and Ce mainly increase the CO insertion site, which cause the highest C2+ alcohol content in the total alcohols over CMF-Mn catalyst and higher total alcohol selectivity over CMF-Zr and CMF-Ce catalyst.

#### 4. Conclusions

Mn, Zr, and Ce additives all could promote the total alcohol selectivity of catalysts in the higher alcohol synthesis from syngas through facilitating the formation of octahedrally coordinated Cu species. It is found that amount of octahedrally coordinated Cu species have a linear relationship with the alcohol selectivity of the catalysts, indicating that more octahedrally coordinated Cu species favor for the alcohol synthesis. However, the three additives behave differently with respect to the interaction among the active components and a triple-active-site model is built to explain the different promoting effects of the three additives. Mn additive facilitates the stronger interaction between Cu and Fe compares to the catalyst without any additives so that promote the formation of higher alcohols. On the contrary, the addition of Zr and Ce weakens the interaction between the active components but increases the possibility of contact between Cu and Fe, which promotes the total alcohol selectivity of catalysts while the C2+ alcohol content in the total alcohols decreases.

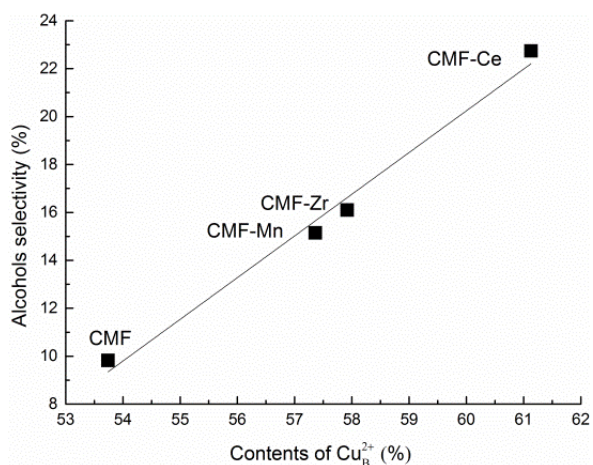


Fig. 7 Relationship between alcohol selectivity and copper content

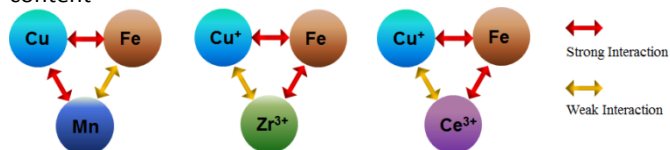


Fig. 8 Scheme illustration of the promoting effects

#### Acknowledgements

The authors acknowledge the financial support from the National High Technology Research and Development Program of China (Nos. 2012AA051002), the Strategic Priority Research Program of the Chinese Academy of Sciences (Nos. XDA01020304), and the projects of National Natural Science Foundation of China (Nos. 21473230).

## Notes and references

- 1 O. Levenspiel, *Ind. Eng. Chem. Res.*, 2005, **44**, 5073-5078.
- 2 P. Johnston, G. J. Hutchings, N. J. Coville, K. P. Finch and J. R. Moss, *Appl. Catal. A: Gen.*, 1999, **186**, 245-253.
- 3 Y. Y. Liu, K. Murata, M. Inaba, I. Takahara and K. Okabe, *J. Jpn. Pet. Inst.*, 2010, **53**, 153-159.
- 4 G. Yang, X. San, N. Jiang, Y. Tanaka, X. Li, Q. Jin, K. Tao, F. Meng and N. Tsubaki, *Catal. Today*, 2011, **164**, 425-428.
- 5 Y. Liu, K. Murata, M. Inaba, I. Takahara and K. Okabe, *Fuel*, 2013, **104**, 62-69.
- 6 M. Gupta, V. Schwartz, S. H. Overbury, K. More, H. M. Meyer and J. J. Spivey, *J. Phys. Chem. C*, 2012, **116**, 10924-10933.
- 7 M. Lin, K. Fang, D. Li and Y. Sun, *Catal. Commun.*, 2008, **9**, 1869-1873.
- 8 M. Ding, J. Liu, Q. Zhang, N. Tsubaki, T. Wang and L. Ma, *Catal. Commun.*, 2012, **28**, 138-142.
- 9 W. Gao, Y. Zhao, J. Liu, Q. Huang, S. He, C. Li, J. Zhao and M. Wei, *Catal. Sci. Technol.*, 2013, **3**, 1324-1332.
- 10 L. Zhao, K. Fang, D. Jiang, D. Li and Y. Sun, *Catal. Today*, 2010, **158**, 490-495.
- 11 N. Wang, K. Fang, D. Jiang, D. Li and Y. Sun, *Catal. Today*, 2010, **158**, 241-245.
- 12 D. Mei, R. Rousseau, S. M. Kathmann, V.-A. Glezakou, M. H. Engelhard, W. Jiang, C. Wang, M. A. Gerber, J. F. White and D. J. Stevens, *J. Catal.*, 2010, **271**, 325-342.
- 13 R. P. UNDERWOOD and A. T. BELL, *J. Catal.*, 1988, **109**, 61-75.
- 14 Y. W. Lu, F. Yu, J. Hu and J. Liu, *Appl. Catal. A: Gen.*, 2012, **429**, 48-58.
- 15 W. Gao, Y. Zhao, J. Liu, Q. Huang, S. He, C. Li, J. Zhao and M. Wei, *Catal. Sci. Technol.*, 2013, **3**, 1324-1332.
- 16 W. Gao, Y. Zhao, H. Chen, H. Chen, Y. Li, S. He, Y. Zhang, M. Wei, D. G. Evans and X. Duan, *Green Chem.*, 2014, DOI: 10.1039/c4gc01633e.
- 17 M. Ding, J. Tu, J. Liu, N. Tsubaki, T. Wang and L. Ma, *Catal. Today*, 2014, **234**, 278-284.
- 18 J. M. Beiramar, A. Griboval-Constant and A. Y. Khodakov, *ChemCatChem*, 2014, **6**, 1788-1793.
- 19 D. S. Mao, Q. S. Guo, J. Yu, L. P. Han and G. Z. Lu, *Acta Phys. Chim. Sin.*, 2011, **27**, 2639-2645.
- 20 Y. Xiang, V. Chitry, P. Liddicoat, P. Felfer, J. Cairney, S. Ringer and N. Kruse, *J. Am. Chem. Soc.*, 2013, **135**, 7114-7117.
- 21 J. Wang, P. A. Chernavskii, Y. Wang and A. Y. Khodakov, *Fuel*, 2013, **103**, 1111-1122.
- 22 R. Xu, W. Wei, W. Li, T. Hu and Y. Sun, *J. Mol. Catal. A: Chem.*, 2005, **234**, 75-83.
- 23 Z. Yuan, L. Wang, J. Wang, S. Xia, P. Chen, Z. Hou and X. Zheng, *Appl. Catal., B: Environ.*, 2011, **101**, 431-440.
- 24 S. Xia, R. Nie, X. Lu, L. Wang, P. Chen and Z. Hou, *J. Catal.*, 2012, **296**, 1-11.
- 25 M. Lenglet, P. Foulatier, J. Düeb and J. Arsène, *physica status solidi (a)*, 1986, **94**, 461-466.
- 26 F. Li, L. Zhang, D. G. Evans and X. Duan, *Colloid Surf. A: Physicochem. Eng. Asp.*, 2004, **244**, 169-177.
- 27 F. Peng, T. Luo and Y. Yuan, *New J. Chem.*, 2014, **38**, 4427-4433.
- 28 H. Zhang, W. Chu, H. Xu and J. Zhou, *Fuel*, 2010, **89**, 3127-3131.
- 29 Y. Z. Xiang, V. Chitry and N. Kruse, *Catal. Lett.*, 2013, **143**, 936-941.
- 30 R. Xu, Z. Y. Ma, C. Yang, W. Wei and Y. H. Sun, *React. Kinet. Catal. Lett.*, 2004, **81**, 91-98.
- 31 M. Gupta and J. J. Spivey, *Catal. Today*, 2009, **147**, 126-132.
- 32 X. Zhu, Y. Du, H. Wang, Y. Wei, K. Li and L. Sun, *J. Rare Earths*, 2014, **32**, 824-830.
- 33 Y. Zhang, M. Yang, X.-M. Dou, H. He and D.-S. Wang, *Environ. Sci. Technol.*, 2005, **39**, 7246-7253.
- 34 F. J. Pérez-Alonso, M. López Granados, M. Ojeda, P. Terreros, S. Rojas, T. Herranz, J. L. G. Fierro, M. Gracia and J. R. Gancedo, *Chem. Mater.*, 2005, **17**, 2329-2339.
- 35 P. Gao, F. Li, H. Zhan, N. Zhao, F. Xiao, W. Wei, L. Zhong, H. Wang and Y. Sun, *J. Catal.*, 2013, **298**, 51-60.